Eur. Phys. J. D (2023)77:72
https://doi.org/10.1140/epjd/s10053-023-00638-0

THE EUROPEAN PHYSICAL JOURNAL D

Regular Article – Atomic Physics

On the importance of using realistic partition functions in kilonova opacity calculations

Helena Carvajal Gallego[1,a], Jérôme Deprince[1,2,b], Michel Godefroid[3,c], Stéphane Goriely[2,d], Patrick Palmeri[1,e], and Pascal Quinet[1,4,f]

[1] Physique Atomique et Astrophysique, Université de Mons, 7000 Mons, Belgium
[2] Institut d'Astronomie et d'Astrophysique, Université Libre de Bruxelles, 1050 Brussels, Belgium
[3] SQUARES, Université Libre de Bruxelles, 1050 Brussels, Belgium
[4] IPNAS, Université de Liège, Sart Tilman, 4000 Liège, Belgium

Received 23 December 2022 / Accepted 16 March 2023

Abstract. In the present work, we report an investigation on the importance of using realistic partition functions in the opacity calculations of lanthanide ions whether they are moderately or lowly ionized. In order to do this, atomic data for various moderately charged samarium (Sm V–XI) and lowly charged neodymium (Nd II–IV) ions were calculated by the pseudo-relativistic Hartree–Fock method (HFR) and then, used to compute the expansion opacities for conditions characterizing the ejecta of kilonovae observed as a result of neutron star mergers, with a particular attention given to the partition function computations.

1 Introduction

On August 17, 2017, the LIGO and VIRGO collaboration detected for the first time the gravitational waves generated by the coalescence of two neutron stars [1]. This event was named GW170817. Such collision is accompanied by the emission of hot and radioactive matter in which take place nuclear reactions leading to the formation of a large amount of atomic species heavier than iron, such as lanthanides [2]. This gigantic and very luminous explosion, known as kilonova, makes it possible to study the origin of these heavy elements. The determination of kilonova light curve strongly depends on the kilonova opacity, which is dominated by the lanthanide opacity [3] because of the superposition of millions of spectral lines resulting from their complex electronic structure due to the unfilled 4f subshell [4]. However, very crude approximations are used for the opacity in kilonova light curve modeling so far [3].

During the last few years, different investigations were focused on atomic data determination in lowly ionized lanthanides such as Nd II-IV [5], Er III [6], Pr-Gd II [7], Ce II-IV [8], La-Lu I-IV [9] and La-Yb I-IV [10] with the aim of estimating opacities for kilonova conditions one day after the neutron star merger, i.e., for temperatures typically below 20,000 K [9]. The study of earlier kilonova phases correspond to higher temperatures and thus, requires the knowledge of atomic and opacity data for charge states above IV. This motivated us to start a systematic investigation of spectroscopic properties for four- to nine-times ionized lanthanides that so far includes the La V–X [11], Ce V–X [12], Pr–Nd–Pm V–X [13] and Nd–Sm–Eu I–XI [14] ions for which new energy levels, wavelengths and oscillator strengths were computed for several millions of spectral lines and used for evaluating the corresponding expansion opacities.

In [4–9,11,12,14], the partition function, $U(T)$, was approximated to the statistical weight of the ground level, g_0, for the computation of the Sobolev optical depth. This approximation has a significant impact on the computed opacities. The main purpose of the present work is to evaluate how it can affect the expansion opacity for a couple of lanthanide examples, namely for samarium (Sm) in the case of early phase kilonova conditions (t = 0.1 day after the merger), which is associated with moderately charged species (Sm V–XI) and for neodymium (Nd) in the case of plausible conditions in the kilonova ejecta that should take place about 1 day after the neutron star merger (NSM), corresponding to the presence of lowly ionized elements in the ejecta (Nd II–IV).

Jérôme Deprince, Michel Godefroid, Stéphane Goriely, Patrick Palmeri, and Pascal Quinet have contributed equally to this work.

[a] e-mail: helena.carvajalgallego@umons.ac.be (corresponding author)
[b] e-mail: jerome.deprince@ulb.be
[c] e-mail: michel.godefroid@ulb.be
[d] e-mail: stephane.goriely@ulb.be
[e] e-mail: patrick.palmeri@umons.ac.be
[f] e-mail: pascal.quinet@umons.ac.be

Published online: 10 May 2023

2 Theoretical approach: pseudo-relativistic Hartree–Fock method (HFR)

In the present work, the pseudo-relativistic Hartree–Fock (HFR) theoretical approach [15] was used to calculate the atomic parameters in Nd and Sm ions required to compute their opacities, as in [10–13,16]. This method, in which the different electronic orbitals are obtained by solving the Hartree–Fock equations deduced from the variational minimization of the average energies for each configuration included in the model and in which one-body relativistic corrections (spin-orbit, mass-velocity and Darwin terms) are considered in a perturbative way, is particularly well suited to produce a very large amount of atomic data.

The construction and diagonalization of the multiconfiguration Hamiltonian matrix is carried out within the framework of the Slater–Condon theory. Each matrix element is computed as a sum of products of Racah angular coefficients, radial Slater and spin-orbit integrals:

$$< a|H|b >= \sum_i c_i^{a,b} I_i^{a,b}. \quad (1)$$

In the Slater–Condon method, the atomic wavefunctions Φ_k are built as a superposition of basis states ϕ_b in the LSJπ representation such as:

$$\Phi_k = \sum_b y_k^b \phi_b, \quad (2)$$

where the mixing coefficients y_k^b have to satisfy the condition:

$$\sum_b (y_k^b)^2 = 1. \quad (3)$$

The eigenvalues and eigenstates obtained can be used to compute the radiative parameters such as wavelengths and oscillator strengths for all transitions.

The multiconfiguration models considered for Sm V–XI and Nd II–IV are, respectively, listed in Tables 1 and 2. For the former, for comparison purpose, the models used in our computations are fully described in [14]. In the case of Nd II–Nd IV, the configurations included in the models were built by considering single electron excitations from the ground configuration to $n = 5, 6, 7, 8$ orbitals as well as a few double electron excitations toward selected $n = 5$ and $n = 6$ subshells, similarly to [16], in which the same models are used for the Nd HFR computations.

3 Opacity calculations

3.1 Expansion formalism

The bound-bound opacities were calculated for Sm V–XI and Nd II–IV by using the whole set of atomic data obtained in this work with the pseudo-relativistic Hartree–Fock method. The opacities were computed in the expansion formalism as described in [17–19], the same formalism that was employed in our recent works on Ce II–IV, La V–X, Ce V–X and Pr–Nd–Pm V–X [8,11–13]. In this formalism, the absorption coefficient is given by:

$$\kappa^{bb}(\lambda) = \frac{1}{\rho ct} \sum_l \frac{\lambda_l}{\Delta\lambda} (1 - e^{-\tau_l}), \quad (4)$$

Table 1 Configurations included in the HFR calculations for Sm V–XI ions

Sm V	Sm VI	Sm VII	Sm VIII	Sm IX	Sm X	Sm XI
$4f^4 5p^6$	$4f^3 5p^6$	$4f^3 5p^5$	$4f^3 5p^4$	$4f^3 5p^3$	$4f^3 5p^2$	$4f^3 5p$
$4f^5 5p^5$	$4f^4 5p^5$	$4f^2 5p^6$	$4f^2 5p^5$	$4f^2 5p^4$	$4f^2 5p^3$	$4f^2 5p^2$
$4f^3 5p^6 6s$	$4f^3 5p^5 6s$	$4f^3 5p^4 6s$	$4f^3 5p^3 6s$	$4f^3 5p^2 6s$	$4f^3 5p6s$	$4f^3 6s$
$4f^3 5p^6 6p$	$4f^3 5p^5 6p$	$4f^3 5p^4 6p$	$4f^3 5p^3 6p$	$4f^3 5p^2 6p$	$4f^3 5p6p$	$4f^3 6p$
$4f^3 5p^6 5d$	$4f^3 5p^5 5d$	$4f^3 5p^4 5d$	$4f^3 5p^3 5d$	$4f^3 5p^2 5d$	$4f^3 5p5d$	$4f^3 5d$
$4f^3 5p^6 7s$	$4f^3 5p^5 7s$	$4f^3 5p^4 7s$	$4f^3 5p^3 7s$	$4f^3 5p^2 7s$	$4f^3 5p7s$	$4f^3 7s$

Table 2 Configurations included in the HFR calculations for Nd II–IV ions

Nd II	$4f^5$, $4f^4 5d$, $4f^4 5f$, $4f^4 5g$, $4f^4 6s$, $4f^4 6p$, $4f^4 6d$, $4f^4 6f$, $4f^4 6g$, $4f^4 7s$, $4f^4 7p$, $4f^4 7d$, $4f^4 7f$, $4f^4 7g$, $4f^4 8s$, $4f^4 8p$, $4f^4 8d$, $4f^4 8f$, $4f^4 8g$, $4f^3 5d^2$, $4f^3 5d6s$, $4f^3 5d6p$, $4f^3 5d6d$, $4f^3 6s^2$, $4f^3 6s6p$, $4f^3 6s6d$
Nd III	$4f^4$, $4f^3 5d$, $4f^3 5f$, $4f^3 5g$, $4f^3 6s$, $4f^3 6p$, $4f^3 6d$, $4f^3 6f$, $4f^3 6g$, $4f^3 7s$, $4f^3 7p$, $4f^3 7d$, $4f^3 7f$, $4f^3 7g$, $4f^3 8s$, $4f^3 8p$, $4f^3 8d$, $4f^3 8f$, $4f^3 8g$, $4f^2 5d^2$, $4f^2 5d6s$, $4f^2 5d6p$, $4f^2 5d6d$, $4f^2 6s^2$, $4f^2 6s6p$, $4f^2 6s6d$
Nd IV	$4f^3$, $4f^2 5d$, $4f^2 5f$, $4f^2 5g$, $4f^2 6s$, $4f^2 6p$, $4f^2 6d$, $4f^2 6f$, $4f^2 6g$, $4f^2 7s$, $4f^2 7p$, $4f^2 7d$, $4f^2 7f$, $4f^2 7g$, $4f^2 8s$, $4f^2 8p$, $4f^2 8d$, $4f^2 8f$, $4f^2 8g$, $4f5d^2$, $4f5d6s$, $4f5d6p$, $4f5d6d$, $4f6s^2$, $4f6s6p$, $4f6s6d$

where ρ (in g cm^{-3}) is the density of the ejecta, c (in cm/s) is the speed of light, t (in s) is the elapsed time since ejection, λ (in Å) is the central wavelength within the region of width $\Delta\lambda$, λ_l are the wavelengths of the lines appearing in this range and τ_l are the corresponding optical depths.

The latter is expressed using the following expression [20]:

$$\tau_l = \frac{\pi e^2}{m_e c} f_l n_l t \lambda_l, \tag{5}$$

where e (in C) is the elementary charge, m_e (in g) is the electron mass, f_l (dimensionless) is the oscillator strength, and n_l (in cm^{-3}) is the density of the lower level of the transition. Since the local thermodynamic equilibrium (LTE) is assumed in this formalism, n_l can be expressed using the Boltzmann distribution according to the statistical weight g_0 and the density n_0 of the ground state as

$$n_l = n_0 \frac{g_l}{g_0} e^{-E_l/k_B T}, \tag{6}$$

where k_B is the Boltzmann constant (in cm^{-1}K^{-1}), T (in K) is the temperature and g_l and E_l (in cm^{-1}) are, respectively, the statistical weight (defined as $g_l = 2J_l + 1$, J_l being the total electronic angular momentum of the atom in the level l) and the energy of the lower level of the transition with respect to the ground level energy of the ion considered.

Summing Eq. 6 over all the levels of the ion, we obtain:

$$n = \sum_{l=0}^{\infty} n_l = \frac{n_0}{g_0} \sum_{l=0}^{\infty} g_l \; e^{-E_l/k_B T}, \tag{7}$$

where n is the ion density, defined according to [21] by the formula

$$n = \frac{\rho}{A m_p} X_j, \tag{8}$$

in which A is the mass number, m_p is the proton mass and X_j is the relative ionic fraction of the j^{th} ionization state. Introducing the partition function $U(T)$ defined as

$$U(T) = \sum_{l=0}^{\infty} g_l \; e^{-E_l/k_B T}, \tag{9}$$

Equation 7 becomes

$$\frac{n_0}{g_0} = \frac{n}{U(T)}. \tag{10}$$

As a consequence, the Boltzmann distribution given in Eq. 6 can be written as

$$n_l = \frac{n}{U(T)} g_l \; e^{-E_l/k_B T}, \tag{11}$$

and therefore, Eq. 5 can be rewritten as:

$$\tau_l = \frac{\pi e^2}{m_e c} \frac{n \lambda_l t}{U(T)} g_l f_l e^{-E_l/k_B T}. \tag{12}$$

At moderate temperatures, the populations of the higher levels are quite small and $U(T)$ may converge rapidly. However, in complex atoms, there may be a large number of low-lying levels that remain appreciably populated even at fairly low temperature. The approximation $U(T) \simeq g_0$, as used in some of our previous works (e.g., [8], see Eq. 5), as well as in [5] (see Eq. 7), in [9] and in other works from this group (as stated in [16]), is therefore inappropriate.

3.2 Influence of partition functions

3.2.1 Moderately ionized lanthanides (Sm V–XI)

In the case of early phase kilonova, for typical conditions of $T > 20\,000$ K, a density $\rho = 10^{-10}$ g cm^{-3} and a time after the merger $t = 0.1$ day, moderately ionized lanthanides (typically between the fifth and the eleventh degree of ionization) are present in the ejecta. In this section, we will focus on samarium ions from Sm V to Sm XI. As it can be seen in Fig. 1, the statistical weight of the ground state (g_0) of Sm VII is obviously constant (in this case, $g_0 = 7$) while the partition function $U(T)$ is growing as the temperature increases. For the typical temperatures encountered in the early phase kilonova, i.e., $T > 20\,000$ K, the values of $U(T)$ are much higher than the values of g_0. For example, the value of $U(T)$ at $T = 20\,000$ K is about 200, while the value of g_0 remains equal to 7. If we increase the temperature, the value of $U(T)$ will differ from the statistical weight of the ground state (independent of the temperature) by a few orders of magnitude (see Fig. 2). Consequently, the use of the approximation $U(T) \simeq g_0$

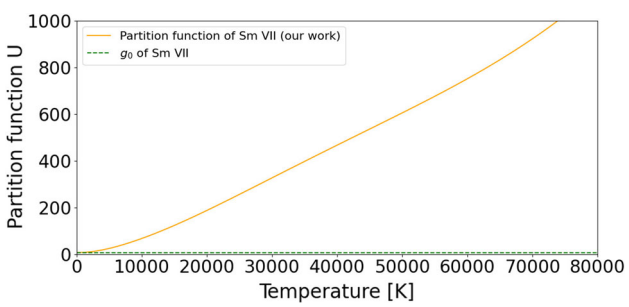

Fig. 1 Partition function $U(T)$ of Sm VII as function as the temperature using the HFR data (orange) and the statistical weight of the ground state ($g_0 = 7$) of Sm VII (green)

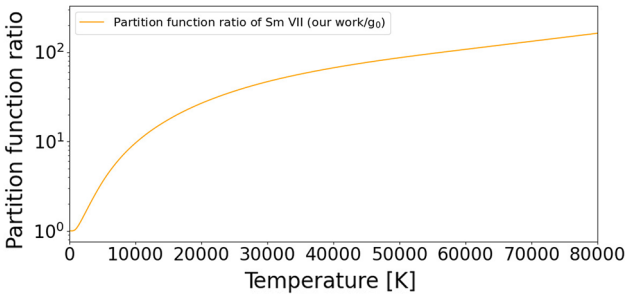

Fig. 2 Partition function ratio (our work/g_0) of Sm VII as function as the temperature

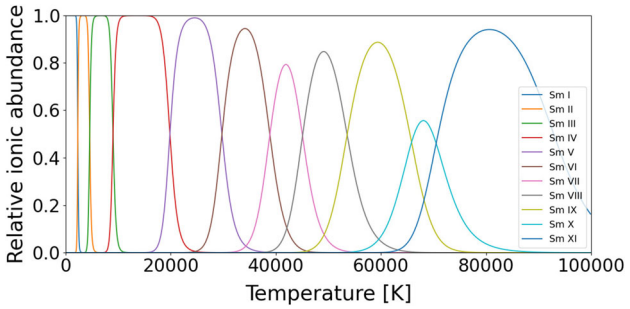

Fig. 3 Relative ionic abundances for Sm I–XI species as a function of temperature

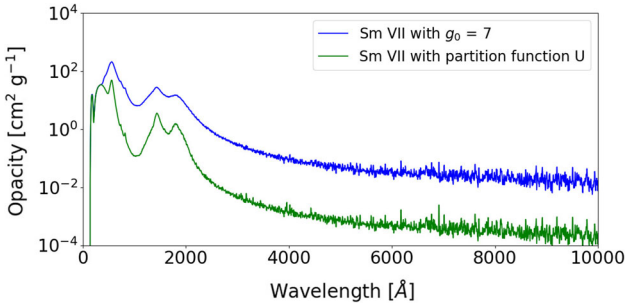

Fig. 4 Expansion opacities for Sm VII calculated with $\rho = 10^{-10}$ g cm^{-3}, $t = 0.1$ d, $T = 42\,000$ K and $\Delta\lambda = 10$ Å using, respectively, the statistical weight of the ground state ($g_0 = 7$) (blue) and the partition function $U(T)$ (green)

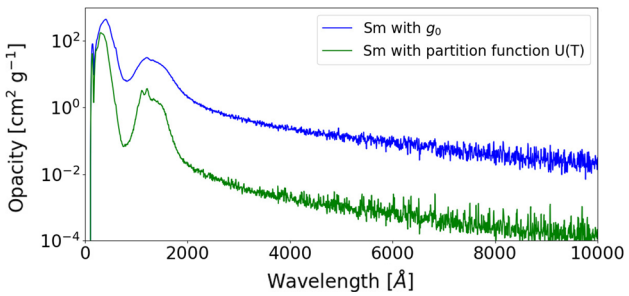

Fig. 5 Expansion opacities for Sm calculated with $\rho = 10^{-10}$ g cm^{-3}, $t = 0.1$ d, $T = 70{,}000$ K and $\Delta\lambda = 10$ Å using, respectively, the statistical weight for the ground state g_0 (blue) and the partition function $U(T)$ (green)

is inadequate for calculating opacities for these ions encountered in the early phase kilonova.

The Samarium ion distribution calculated according to the Saha equations as a function of the temperature is displayed in Fig. 3. Using the atomic data obtained with the HFR method (as explained in Sect. 2), and selecting the temperature $T = 42\,000$ K corresponding to the maximum abundance of Sm VII, the opacity was evaluated for $\rho = 10^{-10}$ g cm^{-3} and $t = 0.1$ day, as shown in Fig. 4. In the latter, both opacities are calculated with the same multiconfiguration model (the same configurations as considered in [14] which are detailed in Table 1). The blue curve corresponds to the opacity calculated by approximating the partition function $U(T)$ by g_0, and the green one represents the opacity obtained when using the partition function estimated taking all the energy levels deduced from our HFR calculations. It can be clearly observed that the opacity obtained with this approximation ($U(T) \simeq g_0$) is overestimated by up to two orders of magnitude.

In Fig. 5, we show the opacity computed when considering all the samarium ions (Sm I–XI) with the same conditions for the time after the merger and the density as for the previous figure and with a temperature $T = 70\,000$ K in order to compare with the opacities obtained in [14]. The Sm opacity computed using g_0 instead of $U(T)$ taking our atomic HFR data (blue curve) is in very good agreement with the one calculated with the HULLAC data in [14], using the same multiconfiguration expansions. When calculating opacities of Sm ions with a more realistic partition function $U(T)$ (obtained by taking all the energy levels into account), the opacity decreases by nearly two orders of magnitude in the infrared, showing the importance of properly computing the partition function in the opacity calculations.

3.2.2 Lowly ionized lanthanides (Nd II–IV)

Lowly ionized lanthanides are present in the kilonova ejecta for typical conditions as expected in the AT2017gf0 kilonova [9], the electromagnetic counterpart of GW170817, when the observation started one day after the merger (namely a temperature of about $T = 5000$ K and a density of $\rho = 10^{-13}$ g cm^{-3} at this time). In this section, we will focus on the case of a typical lanthanide, that is neodymium, in its first ionization stages (Nd II–Nd IV).

As in Fig. 1 for Sm VII, Fig. 6 illustrates for Nd III the difference between the realistic computed partition function $U(T)$ that exponentially increases with temperature, with the approximate constant value $U(T) \simeq g_0 = 9$ of the ground level statistical weight ($J = 4$). It is worth highlighting that the partition functions calculated by only using the energy levels available in the NIST atomic database [22] are by far underestimated with respect to a realistically computed partition function where all the levels from our HFR computation are used, showing that the energy level data available at NIST are not sufficient to compute the partition func-

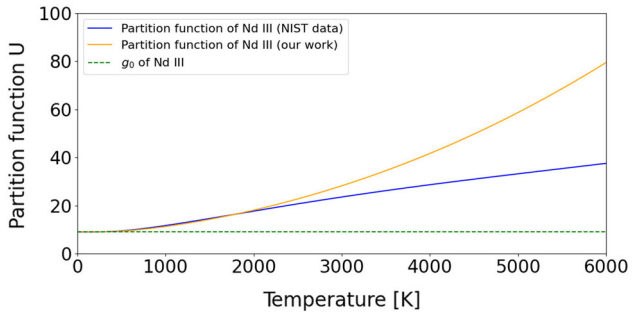

Fig. 6 Evolution of partition function of Nd III with the temperature using, respectively, the levels available at the NIST (blue), the ones from our work (HFR data) (orange) and the statistical weight of the ground state (g_0) of Nd III (green)

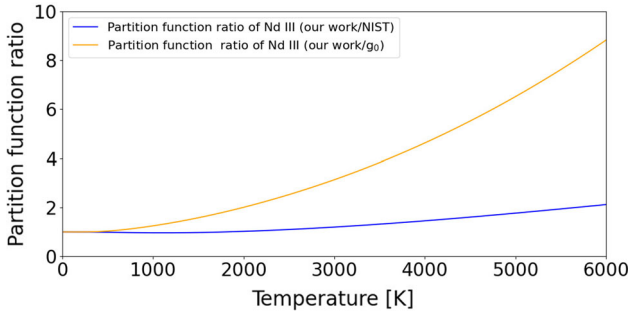

Fig. 7 Evolution of the partition function ratio of Nd III with the temperature (our work/NIST) in blue and (our work/g_0) in orange

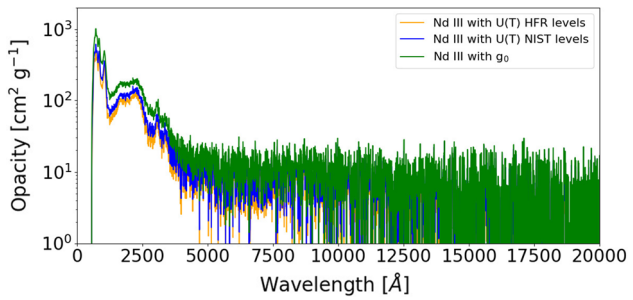

Fig. 8 Expansion opacities for Nd III calculated with $\rho = 10^{-13}$ g cm^{-3}, $t = 1$ d, $T = 5000$ K and $\Delta\lambda = 10$ Å using, respectively, the partition function using the NIST data (blue), the partition function from HFR data (orange) and the statistical weight of the ground state g_0 (green)

tion of Nd III in a realistic way. The difference between the partition function computed in our work and the statistical weight of the ground level can be estimated from Fig. 7, which reveals a realistic partition function value that is about 6 times greater than g_0 at $T = 5000$ K. The impact of such an approximation on the computed opacity is obviously less important than in the case of moderately charged ions (see Sect. 3.2.1) since the temperature is lower (and so the difference between $U(T)$ and g_0 is less important for such temperature, even if it is still significant as shown above).

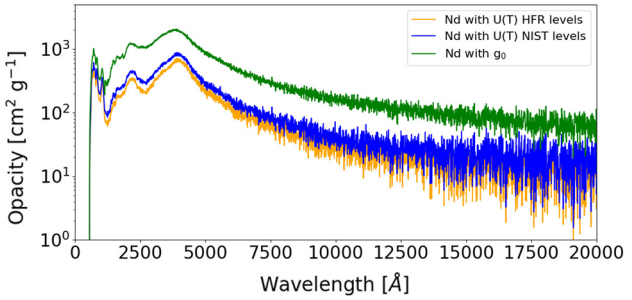

Fig. 9 Expansion opacities for Nd calculated with $\rho = 10^{-13}$ g cm^{-3}, $t = 1$ d, $T = 5000$ K and $\Delta\lambda = 10$ Å using, respectively, the partition function with the NIST data (blue), the partition function with HFR data (orange) and the statistical weight of the ground state g_0 (green)

However, it is noticeable for Nd III, as it can be seen in Fig. 8 and even more significant for the Nd total opacity (due to all the ionization stages), since the opacity is over-estimated by up to a factor of 3 in the latter case when $U(T)$ is replaced by g_0 (Fig. 9). As a result, the computation of atomic expansion opacities in these conditions also requires the partition function to be fully and realistically computed by taking into account all of the computed energy levels, not only the ground level. However, the over-estimation of the opacity due to the consideration of the partition function estimated with the energy levels from the NIST atomic database only is relatively less important.

4 Conclusion

In order to highlight the inadequacy of the commonly used approximation of limiting the partition function to the ground level degeneracy, opacities were calculated for moderately charged samarium and lowly ionized neodymium ions corresponding, respectively, to the lanthanide species expected to be present in a kilonova ejecta in its early phase and from one day after the merger. For this purpose, the HFR method was used to compute the atomic structure and radiative data for Sm V–XI and Nd II–IV. This allowed us to determine a consistent set of theoretical energy levels, radiative wavelengths, transition probabilities, and oscillator strengths for a very large number of spectral lines. All the HFR atomic data were then used to compare the expansion opacities for Sm V–XI and Nd II–IV evaluated with, on the one hand, a realistic evaluation of the partition function in which all the computed energy levels are considered and, on the other hand, a commonly used approximation, namely $U(T) \simeq g_0$, that consists in taking for it the temperature-independent statistical weight of the ground level. Either in the case of lowly charged or moderately charged lanthanide ions, we showed that the use of realistic partition functions in kilonova opacity calculations leads to significant deviation from the approximation consisting in the use of

ground level statistical weight, as commonly assumed in many previous works. We conclude that the use of such a crude approximation over-estimates the opacity in both cases, in particular in the case of moderately charged lanthanides for which the difference reaches two orders of magnitude. For lower temperatures corresponding to lowly charged lanthanides, the differences remain significant. Therefore, a full computation of a realistic partition function in which all the computed energy levels are included is crucial to model at best the kilonova opacity.

Acknowledgements HCG is a holder of a FRIA fellowship, while PP and PQ are, respectively, Research Associate and Research Director of the Belgian Fund for Scientific Research F.R.S.-FNRS. JD has received funding from the FWO and F.R.S.-FNRS under the Excellence of Science (EOS) programme (Nos. O.0004.22 and O022818F). Computational resources have been provided by the Consortium des Equipements de Calcul Intensif (CECI), funded by the F.R.S. -FNRS under Grant No. 2.5020.11 and by the Walloon Region of Belgium.

Author contributions

All authors contributed equally to the paper.

Data Availability Statement This manuscript has no associated data or the data will not be deposited. [Authors' comment: The aim of the present work being to investigate and discuss the impact of the use of realistic partition functions on opacities, the very numerous atomic parameters obtained in our calculations are not tabulated in this paper. These are available on request from the authors.]

References

1. B.P. Abbott et al., GW170817: observation of gravitational waves from a binary neutron star inspiral. Phys. Rev. Lett. **119**(18), 161101 (2017)
2. D. Kasen, B. Metzger, J. Barnes, E. Quataert, E. Ramirez-Ruiz, Nature **551**, 80–84 (2017)
3. O. Just, I. Kullmann, S. Goriely, A. Bauswein, H.-T. Janka, C.E. Collins, MNRAS **510**, 2820–2840 (2022)
4. M. Tanaka et al., ApJ **852**, 109 (2018)
5. G. Gaigalas, D. Kato, P. Rynkun, L. Radziute, M. Tanaka, ApJS **240**, 29 (2019)
6. G. Gaigalas, P. Rynkun, L. Radziute, D. Kato, M. Tanaka, P. Jönsson, ApJS **248**, 13 (2020)
7. L. Radziute, G. Gaigalas, D. Kato, P. Rynkun, M. Tanaka, ApJS **248**, 17 (2020)
8. H. Carvajal Gallego, P. Palmeri, P. Quinet, MNRAS **501**, 1440 (2021)
9. M. Tanaka, D. Kato, G. Gaigalas, K. Kawaguchi, MNRAS **496**, 1369 (2020)
10. C.J. Fontes, C.L. Fryer, A.L. Hungerford, R.T. Wollaeger, O. Korobkin, MNRAS **493**, 4143 (2020)
11. H. Carvajal Gallego, J.C. Berengut, P. Palmeri, P. Quinet, MNRAS **509**, 6138 (2022)
12. H. Carvajal Gallego, J.C. Berengut, P. Palmeri, P. Quinet, MNRAS **513**, 2302 (2022)
13. H. Carvajal Gallego, J. Deprince, J.C. Berengut, P. Palmeri, P. Quinet, MNRAS **518**, 332–352 (2023)
14. S. Banerjee, M. Tanaka, D. Kato, G. Gaigalas, K. Kawaguchi, N. Domoto, ApJ **934**, 117 (2022)
15. R.D. Cowan, *The Theory of Atomic Structure and Spectra* (California University Press, Berkeley, 1981)
16. A. Flörs, R.F. Silva, J. Deprince, H. Carvajal Gallego, G. Leck, G. Martinez-Pinedo, J.M. Sampaio, B. Amaro, J.P. Marques, S. Goriely, P. Quinet, P. Palmeri, M. Godefroid. arXiv:2302.01780 [astro-ph.HE]
17. H. Karp, G. Lasher, K.L. Chan, E.E. Salpeter, ApJ **214**, 161 (1977)
18. R.G. Eastman, P.A. Pinto, ApJ **412**, 731 (1993)
19. D. Kasen, R.C. Thomas, P. Nugent, ApJ **651**, 366 (2006)
20. V.V. Sobolev, *Moving Envelopes of Stars* (Harvard University Press, Cambridge, 1960)
21. S. Banerjee, M. Tanaka, K. Kawaguchi, D. Kato, G. Gaigalas, Apj **901**, 29 (2020)
22. A. Kramida, Yu. Ralchenko, J. Reader, NIST ASD Team, 2020, NIST Atomic Spectra Database (ver.5.7.1.). https://physics.nist.gov/asd